

Propagating torsional Alfvén waves in thermally active solar plasma

S.A. Belov^{1,2*}, S. Vasheghani Farahani³, N.E. Molevich^{1,2}

¹*Department of Physics, Samara National Research University, Moscovskoe sh. 34, Samara, 443086, Russia*

²*Department of Theoretical Physics, Lebedev Physical Institute, Novo-Sadovaya st. 221, Samara, 443011, Russia*

³*Department of Physics, Tafresh University, Tafresh 39518 79611, Iran*

Accepted XXX. Received YYY; in original form ZZZ

ABSTRACT

The aim of the present study is to shed light on the effects connected with thermal misbalance due to non-equal cooling and heating rates induced by density and temperature perturbations in solar active regions hosting either propagating torsional or shear Alfvén waves. A description for the nonlinear forces connected with Alfvén waves in non-ideal conditions is provided based on the second order thin flux tube approximation. This provides insight on the effects of Alfvén-induced motions on the boundary of thin magnetic structures in thermally active plasmas. The equations describing the process of generating longitudinal velocity perturbations together with density perturbations by nonlinear torsional Alfvén waves are obtained and solved analytically. It is shown that the phase shift (compared to the ideal case) and the amplitude of the induced longitudinal plasma motions against the period of mother Alfvén wave are greater for shear Alfvén waves compared to torsional Alfvén waves although following the same pattern. The difference in the influence of thermal misbalance on the induced velocity perturbations is governed by the plasma- β although its effect is stronger for shear waves. It is deduced that for a harmonic Alfvén driver the induced density perturbations are left uninfluenced by the thermal misbalance.

Key words: MHD – Sun: corona – waves

1 INTRODUCTION

The solar atmosphere acts as a perfect laboratory for wave dynamic studies, especially for magnetohydrodynamic (MHD) waves which are ubiquitous in the solar atmosphere (Nakariakov & Kolotkov 2020; Banerjee et al. 2021). In the present study, we focus on the propagation of the Alfvén wave since Alfvén waves have the potential to explain coronal heating and solar wind acceleration. For instance, there is evidence of upwardly propagating torsional Alfvén waves with the energy flux sufficient to heat the solar corona (Jess et al. 2009; Srivastava et al. 2017) in addition to transferring energy released by solar flares. In particular, Aschwanden & Wang (2020) focused on solar flares and reported torsional oscillations at heights between the solar photosphere up to a maximum of 0.25 solar radii with free energies around 60×10^{23} J which provides insight on the amount of energy transfer due to torsional waves in massive flare events. Torsional Alfvén waves also feature in magnetic reconnection sites (Kohutova, P. et al. 2020; Sabri et al. 2020).

For MHD processes in the solar corona, it is important to account for the interplay of various thermodynamic processes maintaining the corona at reported temperatures. Moreover,

for long-lived corona, continuous cooling and heating processes should be in equilibrium. In a ground breaking work, Field (1965) showed that this thermal equilibrium is unstable under a wide range of conditions. As a result, three types of thermal instabilities can arise: isochoric, isobaric, and isentropic. In order to provoke such instabilities, the thermal balance between cooling and heating processes must experience perturbation. The fact of the matter is that when compressional plasma perturbations induced by MHD waves influence the thermal misbalance the concept of wave-induced thermal misbalance arises. The presence of wave-induced thermal misbalance makes the plasma media active for compressional waves to experience dispersion and amplification (Molevich & Oraevskii 1988; Nakariakov et al. 2017). For the solar corona, it was shown that characteristic times of the wave-induced thermal misbalance are as the order of the observed wave periods (Zavershinskii et al. 2019). The recent review about the wave-induced thermal misbalance in the solar corona is presented by Kolotkov et al. (2021).

Among investigations of the influence of the wave-induced thermal misbalance on MHD waves, the major part is dedicated to the influence on slow waves in solar corona. De Moortel & Hood (2004) investigated the effect of optically thin cooling and constant heating on slow waves and compared it with the effect of thermal conduction. It was shown that the effect of thermal conduction was more pronounced

* E-mail: mr_beloff@mail.ru

for the considered parameters. Nakariakov et al. (2017) considered a weakly nonlinear evolution of slow waves in flux tubes accounting for the thermal conduction and viscosity, and the thermal misbalance. The obtained results indicated that the thermal misbalance could be important for slow wave dynamics in the solar corona, and could be used to explain certain discrepancies between theoretical results and observations. Moreover, Nakariakov et al. (2017) proposed that slow waves could act for the diagnostics of the unspecified coronal heating function before Kolotkov et al. (2020) assumed that the stability of slow and entropy waves can constrain the coronal heating function. For standing slow magnetoacoustic waves in hot coronal loops, the thermal misbalance in the presence of thermal conduction was taken under consideration by Kolotkov et al. (2019), where the damping time associated with the thermal conduction was found to be an order of magnitude higher than the damping time associated with the thermal misbalance. Depending on specific heating and cooling functions, three regimes of slow wave evolution are proposed: acoustic over-stability, suppressed damping, and enhanced damping with damping rate near observational values. Zavershinskii et al. (2019) showed that the thermal misbalance can create quasi-periodic magnetoacoustic slow waves while its heating and cooling timescales dictate their characteristic periods. The estimated damping time of these slow wave trains in the solar corona is between 10 and 100 minutes (Duckenfield et al. 2021).

While thermal misbalance influences the dynamics of magnetoacoustic waves even in the linear regime, the Alfvén wave is only affected in the nonlinear regime which is due to the fact that Alfvén waves are incompressible in the linear regime. However they can generate compressional plasma motions in the nonlinear regime (Hollweg 1971; Vasheghani Farahani et al. 2011). Belov et al. (2021b) showed that compressional plasma motions generated by shear Alfvén waves could be affected by the thermal misbalance. This is reflected by the term which is exponentially dependent on the coordinate along the magnetic field appearing in the expression for the induced longitudinal motions. This term was called the exponential bulk flow. In case of a sinusoidal shear Alfvén wave driver, the amplitude and the phase shift of the induced longitudinal motions become dependent on the driver frequency. Moreover, plasma motions generated by Alfvén waves can interact with the mother Alfvén wave, this interaction which is called self-interaction leads to Alfvén wave steepening (Cohen & Kulsrud 1974; Verwichte et al. 1999; Vasheghani Farahani, S. et al. 2012). The thermal misbalance can affect the self-interaction of shear Alfvén waves leading to changes in the steepening rate and the resulting amplitude of Alfvén waves (Belov et al. 2020, 2021a). The scale of the effects of self-interaction of Alfvén waves in different regions of the solar atmosphere in the presence of a thermal misbalance has been studied by Belov et al. (2020).

In the present paper, a further step is taken to study the nonlinearly induced longitudinal motions due to Alfvén waves when thermal misbalance is associated with the solar plasma magnetic structure. Belov et al. (2021b) studied the nonlinear effects connected with shear Alfvén waves in the presence of thermal misbalance, in particular, the deviations of phase shifts and amplitudes of the induced longitudinal motions. Therefore, the aim here is to compare the phase shifts and

amplitudes of the longitudinal motions induced by the torsional Alfvén wave with the analogous longitudinal motions induced by the shear Alfvén wave, as well as, to check the efficiency of this generation due to various environmental effects like plasma- β , which is directly related to the magnetic field in the solar atmospheric conditions.

In the proceeding section II, the model, equilibrium conditions together with the governing thermal misbalance relations considered in the present study are stated. In section III, the evolutionary equations governing the induced perturbations are obtained. The comparison between the effects of the nonlinear shear and torsional Alfvén wave drivers on the induced perturbations regarding the phase shifts and amplitudes are carried out in section IV. In section V, the conclusions are presented.

2 MODEL AND EQUILIBRIUM CONDITIONS

We use the following set of MHD equations (Priest 2014):

$$\frac{\partial \rho}{\partial t} + \nabla \cdot (\rho \mathbf{v}) = 0, \quad (1)$$

$$\rho \left(\frac{\partial \mathbf{v}}{\partial t} + (\mathbf{v} \cdot \nabla) \mathbf{v} \right) = -\nabla P - \frac{1}{4\pi} \mathbf{B} \times (\nabla \times \mathbf{B}), \quad (2)$$

$$\frac{\partial \mathbf{B}}{\partial t} = \nabla \times (\mathbf{v} \times \mathbf{B}), \quad (3)$$

$$\nabla \cdot \mathbf{B} = 0, \quad (4)$$

$$C_V \rho \left(\frac{\partial T}{\partial t} + (\mathbf{v} \cdot \nabla) T \right) - \frac{k_B T}{m} \left(\frac{\partial \rho}{\partial t} + (\mathbf{v} \cdot \nabla) \rho \right) = -\rho Q(\rho, T), \quad (5)$$

$$P = \frac{k_B}{m} \rho T, \quad (6)$$

where ρ , T , and P respectively represent the density, temperature, and pressure of the plasma, while \mathbf{v} and \mathbf{B} are vectors of the plasma velocity and magnetic field. The Boltzmann constant, the mean mass per volume, and the specific heat capacity at constant volume are respectively shown by k_B , m , and C_V . The term $Q(\rho, T) = L(\rho, T) - H(\rho, T)$ is the generalized heat-loss function (Parker 1953; Field 1965), where $L(\rho, T)$ and $H(\rho, T)$ are the cooling and heating rates, respectively. Under steady-state conditions, we have $Q(\rho_0, T_0) = L(\rho_0, T_0) - H(\rho_0, T_0) = L_0 - H_0 = 0$. We introduce the generalized heat-loss function in the form of $Q(\rho, T)$ due to the following reasons. First, the solar corona is composed of optically thin plasma. Thus, there is no need to solve the radiation transfer equation. As a result, cooling rate due to the radiation can be calculated in the form $L(\rho, T)$ (see Eq. 41 for the exact form) (see for details Dere, K. P. et al. 1997; Zanna et al. 2020). Second, since up-to-date no self-consistent model exists for coronal heating, we also assume it as a function of density and temperature $H(\rho, T)$. This statement is also applicable in the case of impulsive heating if the corresponding timescale is much shorter than the waves timescale. We believe that is a reasonable first step

regarding the influence of plasma heating on wave dynamics. Dependencies of the cooling and heating rates on density and temperature enable the perturbations of thermodynamic variables to create thermal misbalance. The impact on the wave dynamics is of interest in the present study. Equations (1)–(6) are supplemented by the mechanical equilibrium condition on the tube boundary:

$$P + \frac{B^2}{8\pi} = P_{ext}^T, \quad (7)$$

where P_{ext}^T is the sum of gas and magnetic pressures of the external medium that acts on the tube boundary.

By implementing the perturbation theory and investigating the axial symmetric motions ($\partial/\partial\phi = 0$), we have kept terms up to the second order of smallness in the Taylor expansion as

$$\begin{aligned} v_r &\approx \alpha^2 v_{r2} = \tilde{v}_r, \quad v_\phi \approx \alpha v_{\phi1} + \alpha^2 v_{\phi2} = \tilde{v}_\phi, \quad v_z \approx \alpha^2 v_{z2} = \tilde{v}_z, \\ B_r &\approx \alpha^2 B_{r2} = \tilde{B}_r, \quad B_\phi \approx \alpha B_{\phi1} + \alpha^2 B_{\phi2} = \tilde{B}_\phi, \\ B_z &\approx B_0 + \alpha^2 B_{z2} = B_0 + \tilde{B}_z, \quad \rho \approx \rho_0 + \alpha^2 \rho_2 = \rho_0 + \tilde{\rho}, \\ T &\approx T_0 + \alpha^2 T_2 = T_0 + \tilde{T}, \quad P \approx P_0 + \alpha^2 P_2 = P_0 + \tilde{P}, \end{aligned} \quad (8)$$

where $|\alpha| \ll 1$ is a small parameter, subscripts 1 and 2 denote the first and second order perturbations, respectively. In expansion (8), we consider that there are no compressional perturbations of the first order, i.e. there is initially only a torsional Alfvén wave. With this expansion, Eqs. (1)–(6) together with the mechanical equilibrium condition (7) can be written as:

$$\frac{\partial \tilde{\rho}}{\partial t} + \frac{1}{r} \rho_0 \frac{\partial r \tilde{v}_r}{\partial r} + \rho_0 \frac{\partial \tilde{v}_z}{\partial z} = 0, \quad (9)$$

$$\begin{aligned} \rho_0 \frac{\partial \tilde{v}_r}{\partial t} - \frac{1}{r} \rho_0 \tilde{v}_\phi^2 = & - \frac{\partial \tilde{P}}{\partial r} \\ & - \frac{1}{4\pi} \left(\frac{1}{r} \tilde{B}_\phi \frac{\partial r \tilde{B}_\phi}{\partial r} - B_0 \left(\frac{\partial \tilde{B}_r}{\partial z} - \frac{\partial \tilde{B}_z}{\partial r} \right) \right), \end{aligned} \quad (10)$$

$$\rho_0 \frac{\partial \tilde{v}_\phi}{\partial t} = \frac{B_0}{4\pi} \frac{\partial \tilde{B}_\phi}{\partial z}, \quad (11)$$

$$\rho_0 \frac{\partial \tilde{v}_z}{\partial t} = - \frac{\partial \tilde{P}}{\partial z} - \frac{1}{4\pi} \tilde{B}_\phi \frac{\partial \tilde{B}_\phi}{\partial z}, \quad (12)$$

$$\frac{\partial \tilde{B}_r}{\partial t} - B_0 \frac{\partial \tilde{v}_r}{\partial z} = 0, \quad (13)$$

$$\frac{\partial \tilde{B}_\phi}{\partial t} - B_0 \frac{\partial \tilde{v}_\phi}{\partial z} = 0, \quad (14)$$

$$\frac{\partial \tilde{B}_z}{\partial t} + \frac{B_0}{r} \frac{\partial r \tilde{v}_r}{\partial r} = 0, \quad (15)$$

$$\frac{1}{r} \frac{\partial r \tilde{B}_r}{\partial r} + \frac{\partial \tilde{B}_z}{\partial z} = 0, \quad (16)$$

$$C_V \rho_0 \frac{\partial \tilde{T}}{\partial t} - \frac{k_B T_0}{m} \frac{\partial \tilde{\rho}}{\partial t} = -\rho_0 \left(Q_{0\rho} \tilde{\rho} + Q_{0T} \tilde{T} \right), \quad (17)$$

$$\tilde{P} = \frac{k_B}{m} \left(\rho_0 \tilde{T} + \tilde{\rho} T_0 \right), \quad (18)$$

$$\tilde{P} + \frac{B_0}{4\pi} \tilde{B}_z + \frac{1}{8\pi} \tilde{B}_\phi^2 = \tilde{P}_{ext}^T. \quad (19)$$

Note that in Eq. (17), we have $Q_{0T} = \partial Q/\partial T|_{\rho_0, T_0}$, $Q_{0\rho} = \partial Q/\partial \rho|_{\rho_0, T_0}$. The second term on the RHS of Eq. (12) is the nonlinear ponderomotive force which is responsible for the longitudinal induced plasma motions due to the Alfvén wave (Vasheghani Farahani et al. 2011; Vasheghani Farahani, S. et al. 2012; Vasheghani Farahani & Hejazi 2017). Since, in the context of the present study, wave dynamics is considered in the long wavelength limit, we assume perturbations for which the condition $R \ll \lambda$ is fulfilled with R and λ respectively representing the tube radius and characteristic wave length for the density, velocity, and magnetic field perturbations along the tube. This allows implementing the second order thin flux tube approximation (Zhugzhda 1996). Under this approximation, the two dimensional problem can be reduced to a one dimensional problem where the variations in the radial direction are out of the question due to the thin geometry of the flux tube. The Taylor expansions of the physical quantities in the radial direction are (Zhugzhda 1996)

$$\begin{aligned} \tilde{v}_r &\approx V r, \quad \tilde{v}_\phi \approx \Omega r, \quad \tilde{v}_z \approx u, \\ \tilde{B}_r &\approx b_r r, \quad \tilde{B}_\phi \approx J r, \quad \tilde{B}_z \approx b_z + b_{z2} r^2, \\ \tilde{\rho} &\approx \rho, \quad \tilde{T} \approx T, \quad \tilde{P} \approx p + p_2 r^2. \end{aligned} \quad (20)$$

We should mention that from hereafter we imply the parameters introduced in the Taylor series represented by Eq. (20), which must not be mistaken with the full expressions for the quantities expressed in Eqs. (1)–(6). Using the Taylor expansion (20) for Eqs. (9)–(19) and following the same procedure as for (Zhugzhda 1996; Vasheghani Farahani et al. 2011), we can obtain the final governing system as:

$$\frac{\partial \rho}{\partial t} + 2\rho_0 V + \rho_0 \frac{\partial u}{\partial z} = 0, \quad (21)$$

$$\begin{aligned} p + \frac{B_0}{4\pi} b_z - \frac{A_0}{2\pi} \left[\rho_0 \left(\frac{\partial V}{\partial t} - \Omega^2 \right) + \frac{1}{4\pi} \left(J^2 + \frac{1}{2} B_0 \frac{\partial^2 b_z}{\partial z^2} \right) \right] = \\ = \tilde{P}_{ext}^T, \end{aligned} \quad (22)$$

$$\rho_0 \frac{\partial u}{\partial t} = - \frac{\partial p}{\partial z} - \frac{A_0}{4\pi^2} J \frac{\partial J}{\partial z}, \quad (23)$$

$$\rho_0 \frac{\partial \Omega}{\partial t} = \frac{B_0}{4\pi} \frac{\partial J}{\partial z}, \quad (24)$$

$$\frac{\partial J}{\partial t} - B_0 \frac{\partial \Omega}{\partial z} = 0, \quad (25)$$

$$\frac{\partial b_z}{\partial t} + 2V B_0 = 0, \quad (26)$$

$$C_V \rho_0 \frac{\partial T}{\partial t} - \frac{k_B T_0}{m} \frac{\partial \rho}{\partial t} = -\rho_0 \left(Q_{0\rho} \rho + Q_{0T} T \right), \quad (27)$$

$$p = \frac{k_B}{m} (\rho_0 T + \rho T_0). \quad (28)$$

Here, $A_0 = \pi R_0^2$ is the unperturbed tube cross-section. Comparing Eqs. (21)–(28) with the classical second order thin flux tube approximation, one may find an additional nonlinear term on the RHS of Eq. (23) which is absent in the classical approach. To obtain this term, we implemented the expansion of Eq. (20) on Eq. (12) and evaluated it on the tube boundary ($r = R_0$). Under this approach, the term $R_0^2 \partial p_2 / \partial z$ also comes into play. However, we neglect this term in comparison with the term $\partial p / \partial z$, since using the thin flux tube approach implies the condition $R \ll \lambda$ to be fulfilled. As a result, the system obtained can be used on tube boundary (or in small vicinity of the boundary) not in the full tube volume. The set of equations expressed by Eqs. (21)–(28) enables studying a solar plasma cylindrical magnetic structure while experiencing the thermal misbalance. In case of ideal conditions, it is instructive to see (Vasheghani Farahani et al. 2011).

Now that the governing set of equations are described (Eqs. (21)–(28)), the basis for discussing how the thermal misbalance affects the induced plasma motions due to torsional Alfvén waves is provided.

3 PLASMA MOTIONS INDUCED BY TORSIONAL WAVES

Combine Eqs. (24) and (25) to obtain the wave equation for torsional Alfvén waves

$$\hat{D}_A J = 0, \quad \hat{D}_A = \frac{\partial^2}{\partial t^2} - C_A^2 \frac{\partial^2}{\partial z^2}, \quad C_A^2 = \frac{B_0^2}{4\pi\rho_0}. \quad (29)$$

Here, C_A^2 is the square of the Alfvén speed. The form of Eq. (29) shows that there is no influence on Alfvén waves from Alfvén induced motions up to the second order. The full exact solution of Eq. (29) can be represented as $J = J_1(z - C_A t) + J_2(z + C_A t)$, where J_1 and J_2 are arbitrary functions. In our work, we consider only waves propagating in the positive direction. Thus, we have $J = J(\xi)$, where $\xi = z - C_A t$.

Other equations from the system (21)–(28) can be combined to derive equations describing how torsional Alfvén waves induce compressional plasma motions in plasma with the thermal misbalance. Let us focus our attention on longitudinal velocity and density perturbations as it may have implications in the context of Alfvénic winds.

3.1 Longitudinal velocity

It is instructive to write the evolutionary equation based on the combined nonlinear effects and thermal misbalance. Thus, the equation describing the process of generation of longitudinal plasma velocity perturbations by torsional

Alfvén waves has the form as

$$\begin{aligned} \frac{\partial}{\partial t} \left[\rho_0 \hat{D}u + \frac{A_0}{2\pi} C_S^2 \frac{\partial^2}{\partial z \partial t} \left(\frac{J^2}{4\pi} - \rho_0 \Omega^2 \right) + C_S^2 \frac{\partial^2 \hat{P}_{\text{ext}}^T}{\partial z \partial t} + \right. \\ \left. + \frac{A_0}{4\pi^2} \left((C_A^2 + C_S^2) + \frac{A_0}{4\pi} \hat{D}_A \right) \frac{\partial}{\partial t} \left(J \frac{\partial J}{\partial z} \right) \right] + \\ + \frac{1}{\tau_V} \left[\rho_0 \hat{D}Q u + \frac{A_0}{2\pi} C_{SQ}^2 \frac{\partial^2}{\partial z \partial t} \left(\frac{J^2}{4\pi} - \rho_0 \Omega^2 \right) + C_{SQ}^2 \frac{\partial^2 \hat{P}_{\text{ext}}^T}{\partial z \partial t} + \right. \\ \left. + \frac{A_0}{4\pi^2} \left((C_A^2 + C_{SQ}^2) + \frac{A_0}{4\pi} \hat{D}_A \right) \frac{\partial}{\partial t} \left(J \frac{\partial J}{\partial z} \right) \right] = 0, \quad (30) \end{aligned}$$

where, in the first square-bracket term, the notations are introduced as

$$\begin{aligned} \hat{D} &= (C_A^2 + C_S^2) \hat{D}_T + \frac{A_0}{4\pi} \hat{D}_S \hat{D}_A, \\ \hat{D}_S &= \frac{\partial^2}{\partial t^2} - C_S^2 \frac{\partial^2}{\partial z^2}, \quad \hat{D}_T = \frac{\partial^2}{\partial t^2} - C_T^2 \frac{\partial^2}{\partial z^2}, \\ C_S^2 &= \frac{C_P}{C_V} \frac{k_B T_0}{m}, \quad C_P = C_V + \frac{k_B}{m}, \quad C_T^2 = \frac{C_A^2 C_S^2}{C_A^2 + C_S^2}, \end{aligned}$$

and, in the second square-bracket term, where all terms are proportional to the derivatives of the generalized heat-loss function $Q(\rho, T)$, we have

$$\begin{aligned} \hat{D}Q &= (C_A^2 + C_{SQ}^2) \hat{D}_{TQ} + \frac{A_0}{4\pi} \hat{D}_{SQ} \hat{D}_A, \quad \tau_V = \frac{C_V}{Q_{0T}}, \\ \hat{D}_{SQ} &= \frac{\partial^2}{\partial t^2} - C_{SQ}^2 \frac{\partial^2}{\partial z^2}, \quad \hat{D}_{TQ} = \frac{\partial^2}{\partial t^2} - C_{TQ}^2 \frac{\partial^2}{\partial z^2}, \\ C_{SQ}^2 &= \frac{(Q_{0T} T_0 - Q_{0\rho} \rho_0) k_B T_0}{Q_{0T} T_0} \frac{1}{m}, \quad C_{TQ}^2 = \frac{C_A^2 C_{SQ}^2}{C_A^2 + C_{SQ}^2}. \end{aligned}$$

Here, we have introduced sound and tube speeds modified by thermal misbalance, C_{SQ} and C_{TQ} , along with the standard sound and tube speeds, C_S and C_T , for more details see, e.g., (Zavershinskii et al. 2019) for the modified sound speed and (Belov et al. 2021c) for the modified tube speed. We note that τ_V is the characteristic time associated with the thermal misbalance, see (Zavershinskii et al. 2019; Kolotkov et al. 2020) for details.

In both square brackets of Eq. (30), the nonlinear forces connected with the torsional Alfvén wave are present as well as the force connected with the back-reaction of the external media (the term proportional to the \hat{P}_{ext}^T). These nonlinear forces are the magnetic tension force (term proportional to $J^2/4\pi$), the centrifugal force (term proportional to Ω^2), and the ponderomotive force (term proportional to $J \partial J / \partial z$) (see e.g. Vasheghani Farahani et al. 2011). The interplay between these nonlinear forces determines the properties and efficiency of plasma motion generation by torsional Alfvén waves. In case of nonlinear shear Alfvén waves, only the ponderomotive force features in the equation analogues to Eq. (30), see (Belov et al. 2021b).

Eq. (30) looks complicated, but it can be greatly simplified under several assumptions. First of all, we assume the external medium of the magnetic tube to be vacuum in a sense that although the equilibrium total magnetic pressure of the external medium exists but it is not perturbed. This means that we have $\hat{P}_{\text{ext}}^T = 0$. Second, as assumed, we consider only Alfvén waves propagating in the positive direction, thus, it follows from Eqs. (24) and (25) that the magnetic tension and centrifugal forces cancel each other ($J^2/4\pi = \rho_0 \Omega^2$), see also (Vasheghani Farahani et al. 2011). Moreover, it follows from

$J = J(z - C_A t)$ that $\hat{D}_A J^2 = 0$. Thus, for torsional Alfvén waves propagating in one (say positive) direction, only one term connected to the ponderomotive force retains in both square brackets of Equation (30). This term is a function of $\xi = z - C_A t$. It allows us to implement our final assumption, that is $u = u(\xi)$, which makes $\hat{D}_A u = 0$. Note that only the motions induced by the Alfvén is desired in the present study.

The assumptions impose Eq. (30) to transform into

$$\begin{aligned} & \frac{\partial}{\partial t} \left(\rho_0 (C_A^2 + C_S^2) \hat{D}_T u + \frac{A_0}{8\pi^2} (C_A^2 + C_S^2) \frac{\partial^2 J^2}{\partial t \partial z} \right) + \\ & + \frac{1}{\tau_V} \left(\rho_0 (C_A^2 + C_{SQ}^2) \hat{D}_T Q u + \frac{A_0}{8\pi^2} (C_A^2 + C_{SQ}^2) \frac{\partial^2 J^2}{\partial t \partial z} \right) = 0. \end{aligned} \quad (31)$$

Equation (31) describes how torsional Alfvén waves induce longitudinal plasma motions by the ponderomotive force in a plasma structure with the thermal misbalance. The exact solution of Eq. (31) in the form $u = u(\xi)$ for the perturbations induced by propagating torsional Alfvén waves would be

$$\begin{aligned} u &= C e^{\Psi \xi} + K_1 \bar{J}^2 + K_2 e^{\Psi \xi} \int e^{-\Psi \xi} \bar{J}^2 d\xi, \quad (32) \\ \bar{J}^2 &= \frac{R_0^2 J^2}{B_0^2}, \quad \Psi = \frac{1}{C_A \tau_V}, \quad K_1 = \frac{C_A^2 + C_S^2}{2C_A}, \quad K_2 = \frac{C_S^2 - C_{SQ}^2}{2C_A^2 \tau_V}. \end{aligned}$$

The solution expressed by Eq. (32) for torsional waves has the same form as the solution for shear waves (Belov et al. 2021b):

$$\begin{aligned} v_z &= C e^{\Psi \xi} + K_1 \left(\frac{B_x}{B_0} \right)^2 + K_2 e^{\Psi \xi} \int e^{-\Psi \xi} \left(\frac{B_x}{B_0} \right)^2 d\xi, \quad (33) \\ \Psi &= \frac{C_A^2 - C_{SQ}^2}{C_A \tau_V (C_A^2 - C_S^2)}, \quad K_1 = \frac{C_A^3}{2(C_A^2 - C_S^2)}, \\ K_2 &= \frac{C_A^2 (C_S^2 - C_{SQ}^2)}{2\tau_V (C_A^2 - C_S^2)^2}. \end{aligned}$$

It could be noticed that the difference between the cases of torsional and shear Alfvén waves is in the values of the coefficients Ψ , K_1 , and K_2 . More specifically, there is no term $(C_A^2 - C_S^2)$ in the denominator for the case of torsional waves. This is a consequence of the fact that longitudinal motions induced by torsional Alfvén waves are less affected by the value of plasma β (Vasheghani Farahani et al. 2011). Moreover, Scalisi et al. (2021) showed that the longitudinal motions induced by torsional Alfvén waves do not depend on plasma β .

In Eq. (32), C is an arbitrary constant that its value can be obtained from the condition $u|_{\xi=0} = 0$. The dimensionless current density is represented as \bar{J} . As stated for the solution of the shear wave (Belov et al. 2021b), each of the three terms on the RHS of Eq. (32) plays a specific role regarding the induced perturbations due to torsional Alfvén waves. The first term on the RHS of Eq. (32) provides information regarding the exponential bulk flow. The second terms has already featured itself for ideal conditions as it is independent of the thermal misbalance, while the third term on the RHS possesses information regarding the thermal misbalance which would be absent for ideal conditions.

Let us focus on the influence of the thermal misbalance for the case of a sinusoidal torsional Alfvén wave-driver as

$$\bar{J} = \alpha \sin(k\xi) = \alpha \frac{e^{ik\xi} - e^{-ik\xi}}{2i}, \quad (34)$$

where k represents the wave-number of the Alfvén wave and α represents the relative amplitude. Substitution of Eq. (34) in the exact solution (32) yields

$$\begin{aligned} u &= C e^{\Psi \xi} + U_0 - A \cos(2k\xi + \phi_0), \quad (35) \\ C &= \frac{\alpha^2 4\omega^2 \tau_V^2 (C_S^2 - C_{SQ}^2)}{4 C_A (1 + 4\omega^2 \tau_V^2)}, \quad U_0 = \frac{\alpha^2 C_A^2 + C_{SQ}^2}{4 C_A}, \\ A &= \sqrt{A_1^2 + A_2^2}, \quad \phi_0 = \arctan\left(\frac{A_2}{A_1}\right), \\ A_1 &= \frac{\alpha^2 (C_A^2 + C_{SQ}^2) + 4\omega^2 \tau_V^2 (C_A^2 + C_S^2)}{4 C_A (1 + 4\omega^2 \tau_V^2)}, \\ A_2 &= \frac{\alpha^2 2\omega \tau_V (C_{SQ}^2 - C_S^2)}{4 C_A (1 + 4\omega^2 \tau_V^2)}, \end{aligned}$$

where $\omega = C_A k$ is the frequency of the Alfvén wave.

It can be noticed from the expression for constant C in Eq. (35) that the direction of the induced flows is determined by the relation between the squares of the sound and modified sound speeds respectively represented by C_S^2 and C_{SQ}^2 . By taking a further look, it could be deduced that if $C_S^2 > C_{SQ}^2$, then the flow moves in the same direction as the Alfvén wave. This condition corresponds to the condition of isentropic stability $\tau_V (C_S^2 - C_{SQ}^2) > 0$, if $\tau_V > 0$ (Molevich & Oraevskii 1988; Zavershinskii et al. 2020). Thus, in the isentropically stable plasma, the flow is co-directed with the Alfvén wave and oppositely-directed in the isentropically unstable plasma. The same result was obtained for the case of shear waves. However regarding the shear Alfvén wave, direction of the bulk flow depends also on the plasma- β . For the case considered in the present study, there is no dependence on the plasma- β .

Also, it can be noticed that the dependence on frequency arises in the velocity amplitude A of the oscillating part of Eq. 35. The high- and low-frequency limits of the amplitude are

$$A = \begin{cases} A_{\text{hf}} = \frac{\alpha^2 C_A^2 + C_S^2}{4 C_A} & \text{for } \omega |\tau_V| \gg 1, \\ A_{\text{lf}} = \frac{\alpha^2 C_A^2 + C_{SQ}^2}{4 C_A} & \text{for } \omega |\tau_V| \ll 1. \end{cases} \quad (36)$$

It can be seen from Eq. (36) that, when $C_S^2 > C_{SQ}^2$ we have $A_{\text{hf}} > A_{\text{lf}}$. It means that there is a more efficient generation of longitudinal oscillations with shorter periods in the isentropically stable plasma. In the opposite case of isentropic instability, we have $A_{\text{hf}} < A_{\text{lf}}$, which corresponds to more efficient generation of longitudinal oscillations with longer periods.

The final feature, which can be found in Eq. (35), is appearance of the frequency-dependent velocity phase shift ϕ_0 . The presence of a such phase-shift leads to state that the maxima of the induced flow and mother Alfvén waves are no longer coincides. In the isentropically stable plasma, the maxima of induced longitudinal perturbation overtakes the Alfvén wave maxima while they fall behind in the isentropically unstable plasma.

3.2 Density

In this subsection, we are going to investigate the influence of thermal misbalance on the generation of density perturbations. Analogous to Eq. (30), we can derive an equation that governs the density perturbation from the set equations

expressed by Eqs. (21)–(28):

$$\begin{aligned} & \frac{\partial^2}{\partial t^2} \left[\hat{D}\rho - \frac{A_0}{2\pi} \frac{\partial^2}{\partial t^2} \left(\frac{J^2}{4\pi} - \rho_0 \Omega^2 \right) - \frac{\partial^2 \tilde{P}_{\text{ext}}^T}{\partial t^2} - \right. \\ & - \frac{A_0}{4\pi^2} \left(C_A^2 + \frac{A_0}{4\pi} \hat{D}_A \right) \frac{\partial}{\partial z} \left(J \frac{\partial J}{\partial z} \right) \left. \right] + \\ & + \frac{1}{\tau_V} \frac{\partial}{\partial t} \left[\hat{D}_Q \rho - \frac{A_0}{2\pi} \frac{\partial^2}{\partial t^2} \left(\frac{J^2}{4\pi} - \rho_0 \Omega^2 \right) - \frac{\partial^2 \tilde{P}_{\text{ext}}^T}{\partial t^2} - \right. \\ & \quad \left. - \frac{A_0}{4\pi^2} \left(C_A^2 + \frac{A_0}{4\pi} \hat{D}_A \right) \frac{\partial}{\partial z} \left(J \frac{\partial J}{\partial z} \right) \right] = 0. \quad (37) \end{aligned}$$

Equation (37) has the same nonlinear forces as of Eq. (30). Following the same procedure as for the velocity, Eq. (37) could be simplified to

$$\begin{aligned} & \frac{\partial^2}{\partial t^2} \left((C_A^2 + C_S^2) \hat{D}_T \rho - \frac{A_0}{8\pi^2} C_A^2 \frac{\partial^2 J^2}{\partial z^2} \right) + \\ & + \frac{1}{\tau_V} \frac{\partial}{\partial t} \left((C_A^2 + C_{SQ}^2) \hat{D}_{TQ} \rho - \frac{A_0}{8\pi^2} C_A^2 \frac{\partial^2 J^2}{\partial z^2} \right) = 0. \quad (38) \end{aligned}$$

Following the same logic as in the previous subsection for longitudinal plasma velocity, we can look for the solution of Eq. (38) in the form $\rho = \rho(\xi)$. Thus, the exact solution for the density perturbations induced by propagating torsional Alfvén waves would be

$$\rho = \frac{\rho_0}{2} \tilde{J}^2 + K e^{\Psi \xi}. \quad (39)$$

The solution expressed by Eq. (39) consists of two terms. The first term coincides with the solution for ideal plasma (Vasheghani Farahani et al. 2011) while the second term is connected with the mass flow introduced by the thermal misbalance. There is no additional influence of thermal misbalance in comparison to ideal conditions other than this effect. We note that K is an arbitrary constant which is determined from the condition $\rho|_{\xi=0} = 0$, where if the Alfvén driver $J|_{\xi=0}$ is equal to zero, we would have $K = 0$, which means that there would be no mass flow. To state clearer, in case of a sinusoidal driver, we have

$$\rho = \frac{\alpha^2}{4} \rho_0 (1 - \cos(2k\xi)), \quad (40)$$

which shows that for the case of a propagating Alfvén wave driver, the induced mass flow is not affected by the thermal misbalance.

4 COMPARISON BETWEEN SHEAR AND TORSIONAL ALFVÉN DRIVERS

The mass flow generated by the torsional Alfvén wave remains the same as for the case of ideal plasma. Owing to this deduction, in this section, we restrict our attention only on the longitudinal plasma motions generated by torsional Alfvén waves and compare with their corresponding motions generated by shear Alfvén waves for plasma parameters associated with solar coronal conditions.

Before performing our comparison, we specify the heat-loss function as $Q(\rho, T)$. In the solar corona, radiation runs away without interacting with the plasma. This is why we only consider losses due to optically thin plasma radiation expressed as

$$L(\rho, T) = \frac{\rho}{4m^2} \Lambda(T), \quad (41)$$

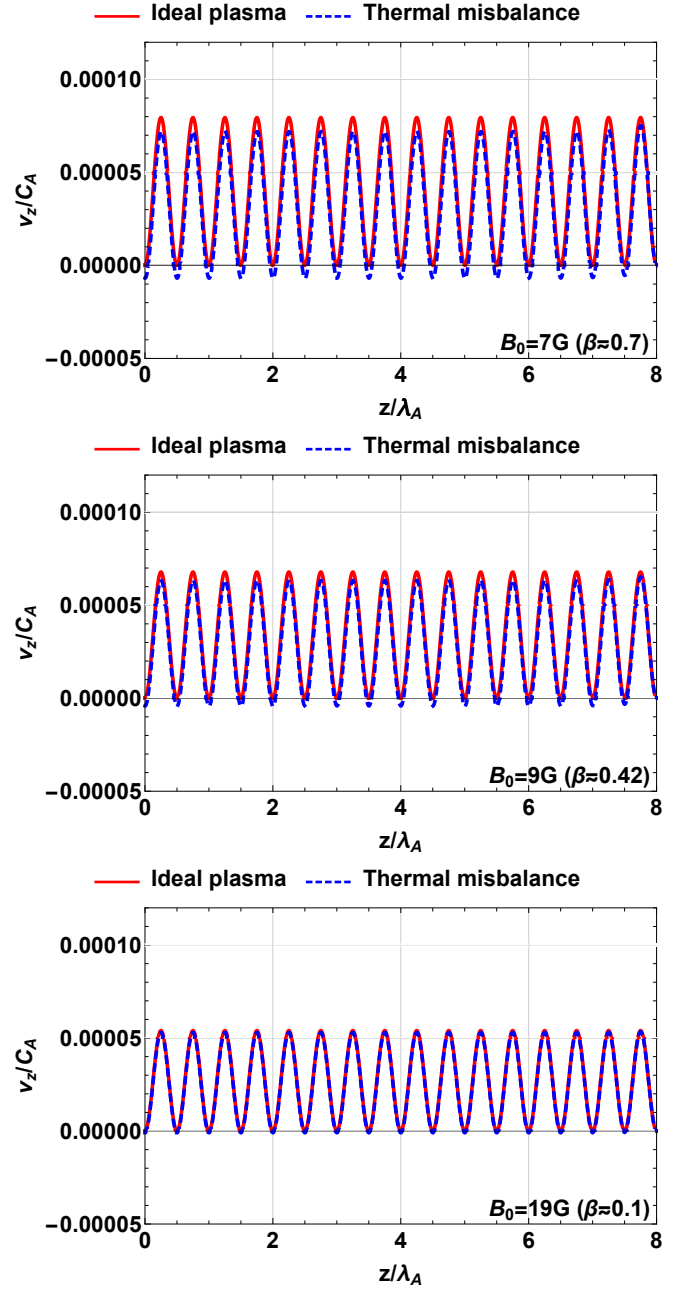


Figure 1. Relative amplitude of longitudinal plasma motion induced by torsional Alfvén waves in plasma with (red curve) and without (dashed-blue curve) thermal misbalance for $T_0 = 1$ MK, $n_e = 5 \times 10^9 \text{ cm}^{-3}$, and $B_0 = 7$ G, 9 G, 19 G. See also Fig. 3 of Belov et al. (2021b).

where $m = 0.6 \cdot 1.67 \cdot 10^{-24} \text{ g}$ is the mean particle mass and $\Lambda(T)$ is the radiative-loss function determined from the CHIANTI atomic database v. 10.0 (Dere, K. P. et al. 1997; Zanna et al. 2020). The heating function $H(\rho, T)$ can be locally modeled as

$$H(\rho, T) = h \rho^a T^b, \quad (42)$$

where h , a , and b are given constants. The constant h is determined from the steady-state condition $Q(\rho_0, T_0) = 0$: $h = L(\rho_0, T_0) / \rho_0^a T_0^b$. The power-law indices a and b could be associated with some specific heating mechanism. Kolotkov et al.

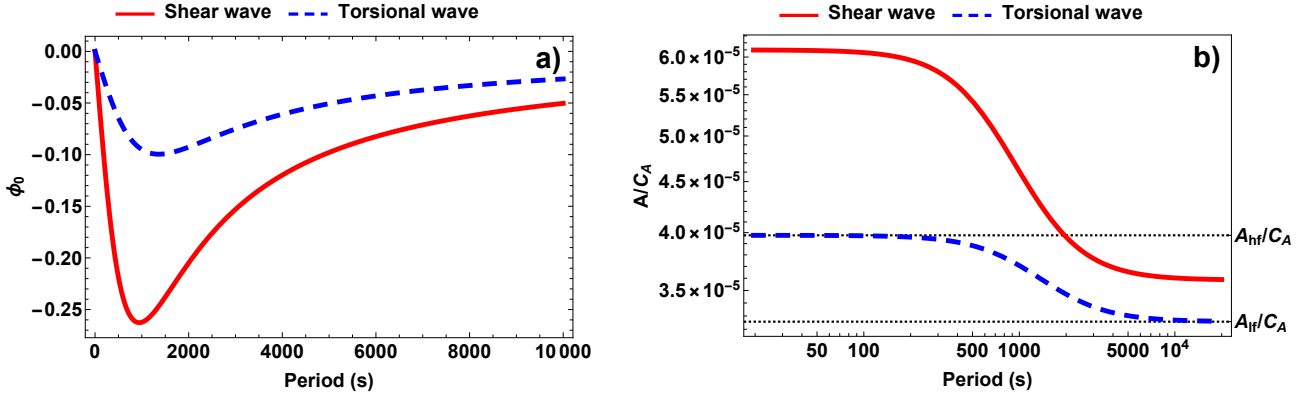


Figure 2. The effects of the Alfvén wave period on two parameters, the phase shift and the amplitude. The red curves correspond to the shear wave driver while the dashed-blue curves correspond to the torsional wave driver. **Panel a)** The phase shift of the oscillating part with respect to ideal plasma conditions regarding longitudinal motions induced by the torsional and shear Alfvén waves, see also Fig. 2 of Belov et al. (2021b). **Panel b)** The relative amplitude of the oscillating part with respect to ideal plasma conditions regarding longitudinal motions induced by the torsional and shear Alfvén waves, see also Fig. 1 of Belov et al. (2021b). Note that we have considered $T_0 = 1$ MK, $n_e = 5 \times 10^9 \text{ cm}^{-3}$, and $B_0 = 7$ G ($\beta \approx 0.7$)

(2020) showed that for a plasma without thermal conduction there is a region of $-2 \lesssim a \lesssim 2.5$ and $-5 \lesssim b \lesssim -3$ where both thermal stability and acoustic stability exist in the coronal plasma. This means that criteria of isochoric, isobaric, and isentropic thermal stability are satisfied for a and b inside this region. In this parameter region, all solutions will be qualitatively the same, the difference will be in the current numerical values of heat-loss function derivatives Q_{0T} and $Q_{0\rho}$, which implies the different values of the induced longitudinal plasma motions. But, once again, the general picture will be qualitatively the same. For example, the exponential bulk flow will be positive for all a and b in this region, but for isentropically unstable plasma, it will be negative. For illustrative purposes, we follow Kolotkov et al. (2020) and also choose the point $a = 1/2$, $b = -7/2$ inside this parameter region. We should mention that the calculations which will be provided in the proceeding are valid for the chosen region of parameters. However, the variation of the heating mechanism will lead to the change the calculated values.

To highlight the influence of thermal misbalance on the induced plasma motions, we plot in Figure 1 the longitudinal plasma motion induced by torsional Alfvén waves in plasma with and without thermal misbalance for Alfvén wave period $P_A = 300$ seconds and different plasma β values. Also, we assume the plasma with temperature $T_0 = 1$ MK, electron number density $n_e = 5 \times 10^9 \text{ cm}^{-3}$ which can correspond to the active region fan loop. It should be mentioned that we start from the relatively higher values of $\beta \approx 0.7$ because, according to (Gary 2001; Bourdin 2017), we can expect $\beta \sim 1$ at relatively low coronal heights: at 140 Mm for (Gary 2001) and at 50 Mm for (Bourdin 2017). We limit ourselves by only plotting the longitudinal velocity, because as we have shown, there should be no thermal misbalance influence on density perturbations for sinusoidal Alfvén driver, and moreover, in the present paper, we do not consider any influence from induced plasma motions on mother Alfvén waves. As can be seen from Figure 1, the main difference between these two cases is the appearance of negative values of the induced velocity perturbation. Also, there is small, but observable, "floating" of peaks in the case of thermal misbalance. These

peaks are "floating up" due to the exponential bulk flow appeared because of the action of thermal misbalance. The same effect was investigated for the case of shear mother Alfvén wave (Belov et al. 2021b). For the plasma β decrease, the difference between plasma with and without thermal misbalance becomes less noticeable.

As obtained in subsection 3.1, the oscillating part of the induced longitudinal plasma motion exhibits a phase shift with respect to the case of ideal plasma (see ϕ_0 in Eq. (35)). This phase shift is dependent on the frequency of the Alfvén wave driver. Plasma motions generated by shear Alfvén waves also experience the frequency dependent phase shift. Figure 2a compares this dependency for the case of shear and torsional Alfvén wave drivers. It can be readily noticed that for the case of torsional wave driver, the phase shift is much smaller, but the dependence is qualitatively the same as for the case of shear driver. It is instructive to compare the efficiency of the oscillating motion generated by torsional and shear Alfvén waves. Thus, we examine value of the amplitude of the oscillating part A from Eq. (35) and compare it with the corresponding value for the case of shear wave driver, see Eq. (13) of Belov et al. (2021b). Figure 2 demonstrates this comparison where, as well as for the phase shift, the amplitude of the plasma motion induced is less for the case of the torsional Alfvén driver. This means that torsional Alfvén waves are less efficient for the generation of oscillating longitudinal plasma motions in comparison to shear waves.

Figure 3 compares the full profile of the induced plasma motion obtained from Eq. (35) with the profile for the case of shear driver for different values of the plasma- β when the Alfvén wave period is set at $P_A = 300$ seconds. For the case where $\beta \approx 0.7$, as was expected from the results, the plasma motion induced by torsional waves experiences a less phase-shift while observing a smaller amplitude than the motion induced by shear waves. Moreover, the exponential bulk flow is almost negligible. The difference between the relative values of the longitudinal plasma motions induced by torsional and shear waves is negligible for $\beta \lesssim 0.1$. In other words, the divergence between the induced amplitudes by the shear and torsional drivers are more pronounced for higher plasma- β

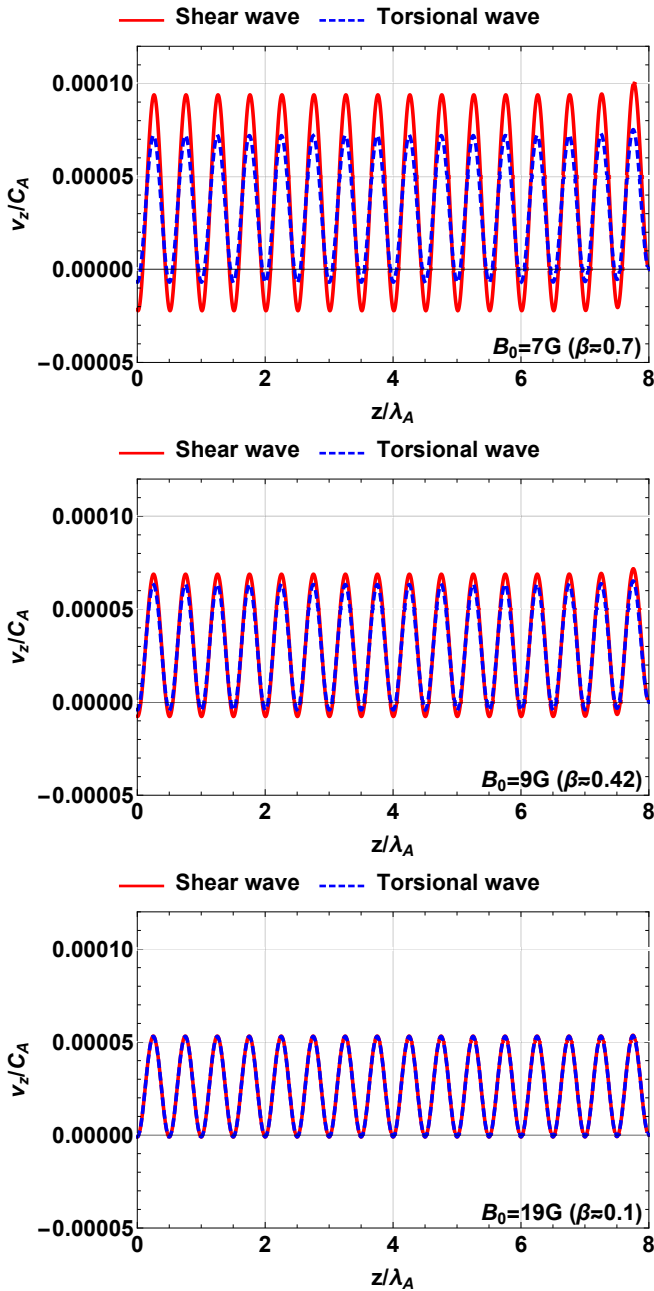


Figure 3. Relative amplitude of longitudinal plasma motion induced by shear (red curve) and torsional (dashed-blue curve) Alfvén drivers for $T_0 = 1$ MK, $n_e = 5 \times 10^9 \text{ cm}^{-3}$, and $B_0 = 7$ G, 9 G, 19 G. See also Fig. 3 of [Belov et al. \(2021b\)](#).

conditions. Thus, the efficiency of the thermal misbalance in inducing higher amplitude perturbations increases with the plasma- β . Moreover, the thermal misbalance although affects the longitudinal motions induced by torsional Alfvén waves, but its influence is less than for the case of shear wave Alfvén wave drivers. This is because of the geometrical difference between torsional and shear Alfvén wave drivers. Due to the axial symmetry, torsional waves produce less influence on plasma. For example, [Vasheghani Farahani et al. \(2011\)](#) showed that for propagating torsional Alfvén waves, the efficiency of the nonlinear generation of compressible perturbations does not grow with the plasma- β as for the case of shear

waves. This result determines, why the influence of thermal misbalance is weaker for torsional Alfvén waves: there is no influence of plasma- β , and all this influence is due to appearance of the sound speed modified by the effect of thermal misbalance.

5 CONCLUSIONS

In this work, the generation of longitudinal plasma motions by torsional Alfvén waves in thermally active plasma has been considered. For this purpose, a mathematical model describing nonlinear Alfvén waves and Alfvén-induced motions on the boundary of thin magnetic flux tube has been derived. In this approach, equations describing the process of generating longitudinal velocity perturbations together with density perturbations by nonlinear torsional Alfvén waves have been highlighted by obtaining and writing the corresponding evolutionary equation together with its solution.

It has been demonstrated that for the case of torsional Alfvén waves the influence of thermal misbalance on the induced longitudinal plasma motion has the same features as for the case of shear Alfvén waves. An important feature in this regard is the presence of an exponential bulk flow besides the appearance of frequency-dependent velocity phase shifts. Another interesting aspect is that the velocity amplitude of the oscillating part of the induced motions is frequency-dependent, see also ([Belov et al. 2021b](#)). Comparison with the case of the shear wave-driver for coronal conditions has revealed the fact that the efficiency of the thermal misbalance is less pronounced for torsional Alfvén waves. In addition, the efficiency of the thermal misbalance is more pronounced on the induced longitudinal motions for higher plasma- β conditions although it features stronger for nonlinear shear Alfvén waves.

Nonlinear torsional Alfvén waves induce density perturbations in ideal conditions ([Vasheghani Farahani et al. 2011](#)). In the case of thermal misbalance, there appears an additional mass flow. However, for a wide class of wave-drivers, where Alfvén perturbations equal zero at the wave front, there is no mass flow and thus, the thermal misbalance does not significantly affect the density perturbations induced by Alfvén waves.

The intriguing result of this work is the difference in influence of the thermal misbalance on plasma velocity and density perturbations. The perturbation of density can even experience no influence due to the thermal misbalance. However, the obtained difference between induced velocity and density perturbations may be the result of simplicity of the model considered, i.e. due to not accounting for higher terms in radial expansion which could be crucial for the dynamics description. To provide a precise answer in this regard, we are motivated to consider more exact 2.5D models as in ([Scalisi et al. 2021](#)) because it describes Alfvén perturbations without any restrictions on the wavelength.

ACKNOWLEDGEMENTS

The study was supported in part by the Ministry of Education and Science of Russia by State assignment to educational and research institutions under Project No. FSSS-

2020-0014 and No. 0023-2019-0003, and by RFBR, project number 20-32-90018. CHIANTI is a collaborative project involving George Mason University, the University of Michigan (USA), University of Cambridge (UK) and NASA Goddard Space Flight Center (USA).

Zavershinskii D. I., Kolotkov D. Y., Nakariakov V. M., Molevich N. E., Ryashchikov D. S., 2019, *Phys Plasmas*, 26, 082113
 Zavershinskii D. I., Molevich N. E., Riashchikov D. S., Belov S. A., 2020, *Phys. Rev. E*, 101, 043204
 Zhugzhda Y. D., 1996, *Phys Plasmas*, 3, 10

This paper has been typeset from a $\text{\TeX}/\text{\LaTeX}$ file prepared by the author.

DATA AVAILABILITY

The data underlying this article will be shared on reasonable request to the corresponding author.

REFERENCES

Aschwanden M. J., Wang T., 2020, *ApJ*, 891, 99
 Banerjee D., et al., 2021, *Space Sci. Rev.*, 217, 76
 Belov S. A., Molevich N. E., Zavershinskii D. I., 2020, *Solar Physics*, 295
 Belov S. A., Molevich N. E., Zavershinskii D. I., 2021a, *Radiophysics and Quantum Electronics*, 63, 694
 Belov S., Vasheghani Farahani S., Molevich N., Zavershinskii D., 2021b, *Solar Physics*, 296, 98
 Belov S. A., Molevich N. E., Zavershinskii D. I., 2021c, *Solar Physics*, 296, 122
 Bourdin P.-A., 2017, *The Astrophysical Journal*, 850, L29
 Cohen R. H., Kulsrud R. M., 1974, *Physics of Fluids*, 17, 2215
 De Moortel I., Hood A. W., 2004, *A&A*, 415, 705
 Dere, K. P. Landi, E. Mason, H. E. Monsignori Fossi, B. C. Young, P. R. 1997, *Astron. Astrophys. Suppl. Ser.*, 125, 149
 Duckenfield T. J., Kolotkov D. Y., Nakariakov V. M., 2021, *A&A*, 646, A155
 Field G. B., 1965, *Astrophys. J.*, 142, 531
 Gary G. A., 2001, *Solar Physics*, 203, 71
 Hollweg J. V., 1971, *J. Geophys. Res.*, 76, 5155
 Jess D. B., Mathioudakis M., Erdélyi R., Crockett P. J., Keenan F. P., Christian D. J., 2009, *Science*, 323, 1582
 Kohutova, P. Verwichte, E. Froment, C. 2020, *A&A*, 633, L6
 Kolotkov D. Y., Nakariakov V. M., Zavershinskii D. I., 2019, *A&A*, 628, A133
 Kolotkov D. Y., Duckenfield T. J., Nakariakov V. M., 2020, *A&A*, 644, A33
 Kolotkov D. Y., Zavershinskii D. I., Nakariakov V. M., 2021, *Plasma Physics and Controlled Fusion*, 63, 124008
 Molevich N. E., Oraevskii A. N., 1988, *Zh. Eksp. Teor. Fiz*, 94, 128
 Nakariakov V. M., Kolotkov D. Y., 2020, *Annu Rev of Astron and Astrophys*, 58, 441
 Nakariakov V. M., Afanasyev A. N., Kumar S., Moon Y.-J., 2017, *The Astrophysical Journal*, 849, 62
 Parker E. N., 1953, *Astrophys. J.*, 117, 431
 Priest E., 2014, *Magnetohydrodynamics of the Sun*. Cambridge University Press, doi:10.1017/CBO9781139020732
 Sabri S., Farahani S. V., Ebadi H., Poedts S., 2020, *Scientific Reports*, 10, 15603
 Scalisi J., Oxley W., Ruderman M. S., Erdélyi R., 2021, *The Astrophysical Journal*, 911, 39
 Srivastava A. K., et al., 2017, *Scientific Reports*, 7
 Vasheghani Farahani S., Hejazi S. M., 2017, *ApJ*, 844, 148
 Vasheghani Farahani, S. Nakariakov, V. M. Verwichte, E. Van Doorselaere, T. 2012, *A&A*, 544, A127
 Vasheghani Farahani S., Nakariakov V. M., Van Doorselaere T., Verwichte E., 2011, *Astron. Astrophys*, 526, A80
 Verwichte E., Nakariakov V. M., Longbottom A. W., 1999, *Journal of Plasma Physics*, 62, 219
 Zanna G. D., Dere K. P., Young P. R., Landi E., 2020, CHIANTI – an atomic database for emission lines – Paper XVI: Version 10, further extensions ([arXiv:2011.05211](https://arxiv.org/abs/2011.05211))